The Persistence of Quantum Coherence in Dipole Dimer States in an Environment of Dipoles: Implications for Photosynthetic Systems?

R A W Bradford
Bennerley, 1 Merlin Haven, Wotton-under-Edge, Glos.GL12 7BA, UK

E-mail : rickatmerlinhaven@hotmail.com

Abstract. Quantum states which retain their coherence for sufficiently long to potentially affect biological processes are currently topical, for example in photosynthesis. It is argued here that, when addressing these issues theoretically, the usual focus on decoherence times may be inappropriate if the system retains non-zero residual coherence in the long term. It is suggested that this could be the generic behaviour for systems whose relevant internal coupling strength (e.g., the Forster coupling) is large compared with the strength of the interaction with the environment. This is illustrated for the case of a dipole dimer interacting with an environment of dipoles. Whilst not intended to be a model of any particular biological system, the illustrative parameters are intended to bear a crude resemblance to photosynthetic units at 300K. The persistence of non-zero coherence is therefore potentially significant.

PACS numbers: 33.15.Kr, 03.65.Yz, 82.50.-m
Keywords: coherence, decoherence, dipoles, photosynthesis
Submitted to: Journal of Physics A: Mathematical and Theoretical

1. Introduction

In the last few years there has been considerable interest in the issue of sustained coherence in the quantum states of biological systems. In part this is due to the observation of quantum beats in photosynthetic systems, [1-7], including at physiological temperatures, [7]. Whilst the duration of the observed quantum coherence is short by everyday standards (e.g., 660 fs at 77K, [3]), it exceeds general expectation prior to 2007. Panitchayangkoon et al, [7], present evidence that quantum coherence survives at physiological temperature for at least 300 fs, long enough to be of relevance to exciton energy transport efficiency. This would not necessarily be via a mechanism analogous to a Grover-type quantum search. In [8-11] it is argued that the highly efficient energy transport in photosynthetic systems arises due to the interplay between the coherent dynamics of the system and the incoherent action of the environment. Nevertheless, sustained coherence is a necessary ingredient, [8-13].

The possibility of coherence being sustained over the required period has been discussed theoretically by many authors, e.g., [8-31], and indeed has been appreciated as a possibility for a very long time (see the historical review by Knox, [14]). Engel and co-workers, [3,7], suggest that the relatively long-lived coherence is the result of the protein infrastructure of the photosynthetic unit taking an active role in the quantum dynamics. Consistent with this, Ishizaki and Fleming, [26-29], have recently produced a decoherence model that takes into account the phonon relaxation dynamics associated with each chromophore in a chromophore-protein complex and have shown that coherence can be sustained for a few picoseconds even at physiological temperatures.

Theoretical studies of decoherence in photosynthetic systems, e.g., [8-31], have generally been based upon some variant of a boson/phonon thermal bath model and/or some variant of a

Redfield/Lindblad type master equation. All these models involve some form of assumed fluctuating field or thermal degrees of freedom which are supposed to simulate the decohering effects of the environment. The reported analyses based on these models generally show a behaviour in which the coherences decay asymptotically to zero. One of the principal outcomes of such models is the characteristic timescale for this decay of coherence.

The purpose of this paper is to point out that the decoherence timescale may not be the most significant issue if, in fact, the decoherence does not proceed to completion. It will be argued that the coherence does not necessarily always decay asymptotically to zero. This is not a new observation. For example, in the context of the decoherence of qubit quantum registers, Reina et al, [32], have shown that at sufficiently low temperatures the coherence saturates to a non-zero value in some cases. Similarly, Jun-Hong An et al, [33], study a model for a pair of optical fields interacting independently with bosonic quantum fields at zero temperature. They also report residual coherence for some parameter values. This can be understood as arising due to non-Markovian behaviour leading to a time-dependent decay rate, and hence to a dynamic evolution of the off-diagonal elements of the density matrix of the form,

$$\frac{\partial \rho_{ab}}{\partial t} \sim \text{unitary part} - \gamma_{ab}(t)\rho_{ab} \tag{1}$$

For suitable parameter values it was found that $\gamma_{ab}(t \to \infty) \to 0$ and hence,

$$LIM_{t\to\infty}\left[\int_0^t \gamma_{ab}(t')dt'\right] \to X \text{ (finite)} \tag{2}$$

which results in ρ_{ab} becoming a non-zero constant, $e^{-X}\rho_{ab}(0)$, at long times (or an oscillation about this non-zero mean). Other authors have also reported slower-than-exponential decays of coherence under suitable circumstances, e.g. Refs.[43-45].

The present paper proposes that the occurrence of non-zero residual coherence is not exotic or pathological, but is actually the generic behaviour in cases where the internal system coupling is strong compared with the coupling to the environment.

The paper is organised as follows. Section 2 discusses in general terms what might be expected as regards decoherence decay, and the possible implications for photosynthetic systems. Section 3 formulates a highly simplified model using a dipole dimer embedded within an environment of dipoles, the purpose of which is to illustrate how non-zero asymptotic coherence results from an analytically tractable approximation. Section 4 refines this model in a number of ways, improving its physical realism to some extent, and presents numerical solutions to this more complex model. However it is emphasised that these toy models are not intended to be taken seriously as models of any particular biological system, having obvious shortcomings. Rather their purpose is only to illustrate the reasonableness of the suggestion that coherence could be ‘permanent’ in systems whose energy spacing exceeds the frequencies available in the environment.

2. Where decoherence leads: the pointer states

Decoherence is often taken to mean that the off-diagonal components of the system’s density matrix reduce to zero so that the density matrix takes the form $\hat{\rho} = \sum_i p_i |i\rangle\langle i|$. However, in general, the density matrix is diagonal only in a particular basis. Transforming to an alternative basis will produce a density matrix with off-diagonal terms. Only if all the probabilities (occupancies), p_i, are equal will the density matrix be diagonal in all bases. So, if interaction with the environment causes decoherence in the sense of making the density matrix diagonal, it must do so with respect to some preferred basis. This has been called the “pointer basis” by Zurek and co-workers, [34-36]. The pointer basis arises, in general, as a result of the dynamics of the system, the environment, and their interaction.

Consider a pair of neighbouring chromophores in a photosynthetic unit, and suppose it suffices to treat each chromophore as having just two states: ground, $|g\rangle$, and a higher energy (excited) state, $|h\rangle$, with energies E_g and E_h respectively. The Hilbert space of the dimer is spanned by the direct product basis states $\{|gg\rangle, |gh\rangle, |hg\rangle, |hh\rangle\}$. This can be called the 'monomer basis' since the energy is clearly located at a specific monomer, e.g. monomer 2 in the case of $|gh\rangle$. But the chromophores are strongly coupled by their mutual dipole Coulomb interaction. Consequently the energy eigenstates of the dimer are linear superpositions of the monomer basis states and define the 'dimer basis', $\{|i\rangle, i \in [0,3]\}$ with energies E_i^d. In the dimer basis states the energy is not spatially localised.

In the context of photosynthetic systems, "decoherence" is usually taken to mean that the energy becomes spatially localised and hence that the density matrix becomes diagonal in the monomer basis. Consequently, the assumption that the coherences vanish after some decoherence time is equivalent to claiming that the pointer basis equals the monomer basis. But why should the pointer basis not be the dimer basis (or something else)? There is an obvious precedent for the energy eigenstates being the pointer basis. Atomic electrons occupy states of well defined energy and are spatially distributed as a consequence. So there is nothing exotic about the suggestion that a pair of chromophores might naturally be einselected to the dimer (energy) basis states.

On the contrary, there appears to be good reason to expect the pointer states for some chromophore dimers to be the energy basis, or at least to involve a large projection onto these basis states. It has been argued by Zurek and Paz, [35], that if the spacing of the energy levels of an

isolated system exceeds the frequencies present in the environment, then the pointer states will approximate to the energy eigenstates of the system. In this limit, the pointer states are not sensitive to the details of the environment or its interaction with the system.

For example, the closest energy levels in a chromophore dimer are the two levels representing a single excitation, which are separated by at least 2Δ, where Δ is the Forster coupling strength. For bacterial light harvesting complexes LHII, the Forster coupling between neighbouring chromophores (monomers comprising single molecules of bacteriochlorophyll, BChl, monomers) is typically in the range 50 – 100 meV, [21, 37]. The spectral density of the environment, in contrast, has been estimated to have a frequency cut-off at $\hbar\omega_c$ between 2 and 8 meV, [21]. The environment of BChl pairs in LHII would therefore appear, according to the criterion of Zurek and Paz, to einselect the energy (dimer) states. Consequently, coherence would be expected to persist in the monomer (spatially localised) basis. This is provided that the diagonal terms, p_i, are not equal, and this is not generally expected.

A second example is the photosynthetic pigment–protein complex, the Fenna–Matthews–Olson (FMO) complex. Based on [38-41], Ishizaki and Fleming, [28], have deployed phonon relaxation times of between 35fs and 166fs. The slowest relaxation is quoted in [28] as corresponding to a frequency cut-off in the spectral density of $\hbar\omega_c = 50\text{cm}^{-1}$ (6 meV). By scaling we take the fastest relaxation as corresponding to $\hbar\omega_c = 240\text{cm}^{-1}$ (30 meV). The same references indicate that the site energy differences along the principal transfer pathways are ~110cm^{-1} (13 meV) or greater. The slowest phonon relaxation rate estimates would therefore again suggest that coherence should persist in the monomer basis, but the FMO case is less clear due to the possibility of faster phonon relaxation.

3. General formulation of the models

This paper considers a dimer composed of a pair of dipole monomers in interaction with an environment which consists of a large number, N, of dipoles. Decoherence is modelled via a direct dipole-dipole Coulomb interaction between the dimer and the environment dipoles

(EDs). The dimer is considered to be prepared in its lowest excited state, the exciton therefore being initially delocalised between the two monomers. The state of the N EDs which comprise the environment is described classically. Hence an environment state is specified by the position and dipole vector for all N EDs.

In the formulation presented below, the state of the environment is assumed to be constant and the dielectric permittivity of the medium between the dipoles is also assumed to be constant. Later, in §5, we attempt to improve on this unphysical idealisation. The time dependent Schrodinger state of the dimer including its interaction with the fixed environment can then be calculated within the 4D Hilbert space of the dimer alone. The reduced density matrix is found by averaging over (tracing-out) an appropriate set of environment states.

The two monomers are assumed to be identical, but in different orientations. Their dipole magnitudes in the ground and excited state are p_g, p_h. All N EDs are assumed to have the same dipole magnitude, *q*, but with relative orientations which are random and uncorrelated. The energy eigenstates of an isolated dimer, in terms of the monomer basis, are given by,

$$\left|i\right\rangle = \sum_{I,J\in\{g,h\}} \alpha_{IJ}^{i} \left|IJ\right\rangle \tag{3}$$

where,

$$E_i^d \alpha_{KL}^i = \left(E_K + E_L\right)\alpha_{KL}^i + \sum_{I,J\in\{g,h\}} \left\langle KL\right|\hat{V}_{\text{dim}}\left|IJ\right\rangle \alpha_{IJ}^i \tag{4}$$

Capital subscripts in (3,4) take the values *g* or *h*, and it is understood that $\left|i\right\rangle$ for $i \in \{0,1,2,3\}$ represents the dimer energy eigenstates in ascending order of dimer energy, E_i^d, where $\hat{H}_{\text{dim}}\left|i\right\rangle = E_i^d \left|i\right\rangle$. Throughout we denote Hilbert space operators by a caret and the free dimer Hamiltonian is $\hat{H}_{\text{dim}}$. Explicitly it is given in the monomer basis by, (5)

$$\left\langle KL\right|\hat{H}_{\text{dim}}\left|IJ\right\rangle = \begin{pmatrix} 2E_g & 0 & 0 & 0 \\ 0 & E_g+E_h & 0 & 0 \\ 0 & 0 & E_g+E_h & 0 \\ 0 & 0 & 0 & 2E_h \end{pmatrix} + \begin{pmatrix} V\left(\vec{p}_{1g},\vec{p}_{2g}\right) & V\left(\vec{p}_{1g},\vec{\mu}_2^*\right) & V\left(\vec{\mu}_1^*,\vec{p}_{2g}\right) & V\left(\vec{\mu}_1^*,\vec{\mu}_2^*\right) \\ V\left(\vec{p}_{1g},\vec{\mu}_2\right) & V\left(\vec{p}_{1g},\vec{p}_{2h}\right) & V\left(\vec{\mu}_1^*,\vec{\mu}_2\right) & V\left(\vec{\mu}_1^*,\vec{p}_{2h}\right) \\ V\left(\vec{\mu}_1,\vec{p}_{2g}\right) & V\left(\vec{\mu}_1,\vec{\mu}_2^*\right) & V\left(\vec{p}_{1h},\vec{p}_{2g}\right) & V\left(\vec{p}_{1h},\vec{\mu}_2^*\right) \\ V\left(\vec{\mu}_1,\vec{\mu}_2\right) & V\left(\vec{\mu}_1,\vec{p}_{2h}\right) & V\left(\vec{p}_{1h},\vec{\mu}_2\right) & V\left(\vec{p}_{1h},\vec{p}_{2h}\right) \end{pmatrix}$$

where the function *V* is the dipole-dipole Coulomb potential energy given by,

$$V\left(\vec{p}_1,\vec{p}_2\right) = \frac{\vec{p}_1\cdot\vec{p}_2 - 3\left(\vec{p}_1\cdot\vec{r}_{12}\right)\left(\vec{p}_2\cdot\vec{r}_{12}\right)}{4\pi\varepsilon_0\varepsilon_{r,12}R_{12}^3} \tag{6}$$

Here $\vec{R}_{12} = \vec{s}_2 - \vec{s}_1$ is the vector distance between the monomers, which are at positions $\vec{s}_1$ and $\vec{s}_2$, and $\vec{r}_{12} = \vec{R}_{12}/R_{12}$ is the corresponding unit vector. The relative permittivity of the medium between the monomers is $\varepsilon_{r,12}$ (set to 2 in all numerical illustrations) whilst ε_0 is the permittivity of the vacuum. The quantities $\vec{\mu}_1, \vec{\mu}_2$, which differ only in orientation, are the transition dipoles of the monomers, defined by,

$$\vec{\mu}_{1,2} = \left\langle h\right|\hat{\vec{\mu}}_{1,2}\left|g\right\rangle \tag{7}$$

where $\hat{\vec{\mu}}_1, \hat{\vec{\mu}}_2$ are the dipole operators for the two monomers whose values in the ground and excited states are $\left\langle g_1\right|\hat{\vec{\mu}}_1\left|g_1\right\rangle = \vec{p}_{1g}$, $\left\langle h_1\right|\hat{\vec{\mu}}_1\left|h_1\right\rangle = \vec{p}_{1h}$, $\left\langle g_2\right|\hat{\vec{\mu}}_2\left|g_2\right\rangle = \vec{p}_{2g}$, $\left\langle h_2\right|\hat{\vec{\mu}}_2\left|h_2\right\rangle = \vec{p}_{2h}$.

We now allow the dimer to interact with a fixed environment state, $\left|e\right\rangle$, so that the dimer eigenstates are changed to $\left|i(e)\right\rangle$ where,

$$\left(\hat{H}_{\dim}+\hat{V}_{env}\right)\left|i(e)\right\rangle\left|e\right\rangle = E_i^{de}\left|i(e)\right\rangle\left|e\right\rangle \tag{8}$$

Here E_i^{de} are the eigen-energies of the dimer including its interaction with the environment via the potential $\hat{V}_{env}$. In the monomer basis, the matrix elements of this interaction potential are,

$$\left\langle IJ\left|\hat{V}_{env}\right|KL\right\rangle = \begin{pmatrix} V_e\left(\vec{p}_{1g},\vec{p}_{2g}\right) & V_e\left(0,\vec{\mu}_2^*\right) & V_e\left(\vec{\mu}_1^*,0\right) & 0 \\ V_e\left(0,\vec{\mu}_2\right) & V_e\left(\vec{p}_{1g},\vec{p}_{2h}\right) & 0 & V_e\left(\vec{\mu}_1^*,0\right) \\ V_e\left(\vec{\mu}_1,0\right) & 0 & V_e\left(\vec{p}_{1h},\vec{p}_{2g}\right) & V_e\left(0,\vec{\mu}_2^*\right) \\ 0 & V_e\left(\vec{\mu}_1,0\right) & V_e\left(0,\vec{\mu}_2\right) & V_e\left(\vec{p}_{1h},\vec{p}_{2h}\right) \end{pmatrix} \tag{9}$$

where the function V_e is the potential energy due to the Coulomb interaction between the dimer and the N EDs, given by,

$$V_e\left(\vec{a},\vec{b}\right) = \sum_{j=1}^{N}\left[\vec{\Phi}_{1j}\left(\vec{a}\right)+\vec{\Phi}_{2j}\left(\vec{b}\right)\right]\cdot\vec{q}_j \tag{10a}$$

where,

$$\vec{\Phi}_{ij}\left(\vec{a}\right) = \frac{\vec{a}-3\left(\vec{a}\cdot\vec{r}_{ij}^{\,e}\right)\vec{r}_{ij}^{\,e}}{4\pi\varepsilon_0\varepsilon_{r,ij}^{e}\left(R_{ij}^{e}\right)^3} \tag{10b}$$

and $\vec{q}_j$ is the dipole vector of the j^{th} ED, $\vec{R}_{ij}^{\,e}$ are their vector positions relative to the i^{th} monomer, and $\vec{r}_{ij}^{\,e} = \vec{R}_{ij}^{\,e}/R_{ij}^{e}$, and $\varepsilon_{r,ij}^{e}$ is the relative permittivity of the medium between the i^{th} monomer and the j^{th} ED. The sum in (10a) extends over all N EDs.

For the convenience of the reader, our notation for the various eigenstates of the dimer is summarised in Table 1.

Basis	Eigen-Energies	Eigen-States
Monomer	$2E_g < E_g + E_h < 2E_h$	$\left\|gg\right\rangle,\left\|gh\right\rangle,\left\|hg\right\rangle,\left\|hh\right\rangle$
Free Dimer	$E_0^d < E_1^d < E_2^d < E_3^d$	$\left\|i\right\rangle, i\in[0,3]$
Dimer-plus-environment	$E_0^{de} < E_1^{de} < E_2^{de} < E_3^{de}$	$\left\|i(e)\right\rangle, i\in[0,3]$

Table 1: Summary of notation for the dimer eigenstates

The dimer is assumed to be prepared in its lowest excited free state, $\left|1\right\rangle$, at t = 0. The initial state of the dimer can therefore be written both in monomer basis and also as an expansion in terms of the eigenstates of (8), thus,

$$\left|1\right\rangle \equiv \sum_{I,J\in\{g,h\}}\alpha_{IJ}^{1}\left|IJ\right\rangle = \sum_{j=0}^{3}A_j\left|j(e)\right\rangle \tag{11a}$$

The coefficients α_{IJ}^{1} follow from solving the eigen-equation (4), and the states $\left|j(e)\right\rangle$, expressed in the monomer basis, follow from solving the eigen-equation (8) using the explicit representations of (5) and (9). Hence the expansion coefficients, A_j, are found from (11a) as,

$$A_j \equiv \sum_{I,J\in\{g,h\}}\left\langle j(e)\right|IJ\rangle\alpha_{IJ}^{1} \tag{11b}$$

The dimer state $\left|s(e,t)\right\rangle$ into which the initial state $\left|1\right\rangle$ evolves then follows from unitary evolution to be,

$$|1\rangle \to |s(e,t)\rangle = \sum_{j=0}^{3} A_j |\, j(e)\rangle \exp\left\{ -i \frac{E_j^{de} t}{\hbar} \right\} \tag{12}$$

The most general mixed state of the environment is $\hat{\rho}_{env} = \sum_{e,e'} p(e,e') |e\rangle\langle e'|$. The density matrix of the dimer-plus-environment at time *t* is thus,

$$\hat{\rho}(t) = \sum_{e,e'} p(e,e') |s(e,t)\rangle\langle s(e',t)| \otimes |e\rangle\langle e'| \tag{13}$$

This is based on the assumption that the environment states can be treated as unaffected by the dimer. An improvement on this (overly simplistic) assumption is considered later (§5). The reduced density matrix for the dimer is obtained by tracing out the environment states, thus,

$$\hat{\rho}^{red}(t) = \sum_{e} p(e,e) |s(e,t)\rangle\langle s(e,t)| \tag{14}$$

Hence, despite the crude idealisation that the environment states can be treated as unaffected by the dimer, nevertheless the reduced density matrix depends upon the whole distribution of states available to the environment (i.e., the fluctuation spectrum) and we shall see that (14) does lead to (at least partial) decoherence.

4. A toy model with an analytic approximation for the coherence

In this first toy model, the set of environment states to be traced-out are specified by allowing all N EDs to have an arbitrary orientation in 3D space, but maintaining their magnitudes and positions fixed. This means that $\sum_{e} p(e,e)...$ in (14) is replaced by $\prod_{i=1}^{N} \left(\frac{1}{4\pi} \int d\Omega_i \right)$, where Ω_i is the solid angle associated with dipole $\vec{q}_i$. This is not at all a realistic model of an aqueous environment but has the advantage of being simple to integrate analytically and provides an algebraic illustration of how residual coherence arises.

A tractable analytic approximation is obtained by assuming the Heitler-London approximation, i.e., that it suffices to consider the dimer state to be within the 2D subspace spanned by $\{|gh\rangle, |hg\rangle\}$ and hence that we can write $|1\rangle = \alpha |gh\rangle - \beta |hg\rangle$. The coefficients α, β are given explicitly by,

$$\beta = \left[1 + \left| \frac{V(\vec{\mu}_1, \vec{\mu}_2^*)}{V(\vec{p}_{1h}, \vec{p}_{2g}) - U_1 + U_2} \right|^2 \right]^{-1/2} \quad \text{and,} \quad \alpha = \frac{V(\vec{\mu}_1, \vec{\mu}_2^*)}{V(\vec{p}_{1h}, \vec{p}_{2g}) - U_1 + U_2} \beta \tag{15}$$

where,
$$U_1 = \left(V(\vec{p}_{1h}, \vec{p}_{2g}) + V(\vec{p}_{1g}, \vec{p}_{2h}) \right) / 2 \tag{16a}$$

and,
$$2U_2 = \left[\left(V(\vec{p}_{1h}, \vec{p}_{2g}) - V(\vec{p}_{1g}, \vec{p}_{2h}) \right)^2 + 4 \left| V(\vec{\mu}_1, \vec{\mu}_2^*) \right|^2 \right]^{1/2} \tag{16b}$$

Note that $2U_2$ is the energy difference between the two distinct singly-excited isolated dimer states, i.e., $2U_2 = E_2^d - E_1^d$, in the Heitler-London approximation. Also note that the term $V(\vec{\mu}_1, \vec{\mu}_2^*) \equiv \Delta$ which occurs in (15,16b) is the Forster coupling of the dimer.

Initially we consider the case of a coupling to the environment which is weak compared with the intra-dimer coupling. To make precise what this means we introduce two quantities, $\Im$ and $\aleph$. The first of these is a measure of the strength of the coupling of the dimer to the

environment and is defined by,

$$\Im = \sum_{j=1}^{N} \vec{P}_j \cdot \vec{q}_j \tag{17}$$

where, $$\vec{P}_j = \alpha\beta\left\{\vec{\Phi}_{1j}\left(\vec{p}_{1g}\right) + \vec{\Phi}_{2j}\left(\vec{p}_{2h}\right) - \vec{\Phi}_{1j}\left(\vec{p}_{1h}\right) - \vec{\Phi}_{2j}\left(\vec{p}_{2g}\right)\right\} \tag{18}$$

where the vector functions $\vec{\Phi}_{ij}$ are defined by (10b). Although $\Im$ is a measure of the strength of the dimer-environment interaction it is not simply the interaction energy because of the minus signs in (18).

The second quantity is a measure of the intra-dimer coupling, essentially a generalisation of the Forster coupling, defined by,

$$\aleph = 2U_2 + \lambda\Im \tag{19}$$

where, $$\lambda = \frac{\beta^2 - \alpha^2}{\alpha\beta} \tag{20}$$

Because of (16b), (19) implies that $\aleph \geq 2U_2 \geq 2\Delta$, so that $\aleph$ is at least as great as twice the Forster coupling.

The utility of these quantities is that the 'weak environment' limit can be defined as $\Im << \aleph$, for which it is sufficient that $\Im << 2\Delta$. In this limit the off-diagonal component of the reduced density matrix is found to be approximated by,

(21)

$$\sum_e \rho_{23} = \rho_{23}^{red} \approx -\alpha\beta + \frac{\alpha\beta}{3U_2^2}\left(1 - \frac{\lambda^2}{4}\right)\sum_{i=1}^{N}\left(P_i\ q_i\right)^2 +$$
$$\left[\prod_{i=1}^{N}\left(\mathrm{sinc}\left(\lambda P_i q_i t\right)\right)\right]\left\{\frac{1}{2U_2}\left[\left(\alpha^2 - \beta^2\right)\sin\left(2U_2 t\right) - i\cos\left(2U_2 t\right)\right]\sum_{j=1}^{N} f_1\left(P_j q_j, \lambda t\right)\right\} +$$
$$\left[\prod_{i=1}^{N}\left(\mathrm{sinc}\left(\lambda P_i q_i t\right)\right)\right]\left\{\frac{1}{U_2^2}\left[\alpha\beta\left(1 - \frac{\lambda^2}{4}\right)\cos\left(2U_2 t\right) + i\frac{\lambda}{4}\sin\left(2U_2 t\right)\right]\left(\sum_{j\neq k}^{N} f_1\left(P_j q_j, \lambda t\right) f_1\left(P_k q_k, \lambda t\right) - \sum_{j=1}^{N} f_2\left(P_j q_j, \lambda t\right)\right)\right\}$$

Here $\mathrm{sinc}(x) = \frac{\sin x}{x}$ and the functions f_1 and f_2 are given by,

$$f_1(x,\xi) = \frac{1}{\mathrm{sinc}(\xi x)}\frac{\partial}{\partial\xi}\left(\mathrm{sinc}(\xi x)\right) \equiv x\cot(\xi x) - \frac{1}{\xi} \tag{22}$$

$$f_2(x,\xi) = -\frac{1}{\mathrm{sinc}(\xi x)}\frac{\partial^2}{\partial\xi^2}\left(\mathrm{sinc}(\xi x)\right) = x^2 + \frac{2x}{\xi}\cot(\xi x) - \frac{2}{\xi^2} \tag{23}$$

Note that the f_1 and f_2 functions have the following limits for short times,

$$Lim\, t \to 0: \qquad f_1(x,\lambda t) \to -\frac{\lambda x t}{3} \tag{24}$$

$$Lim\, t \to 0: \qquad f_2(x,\lambda t) \to +\frac{x^2}{3} \tag{25}$$

When $t = 0$ the product of sinc functions is unity and from (24) the terms involving f_1 are zero. However at $t = 0$ the f_2 term in (21) is non-zero and is equal and opposite to the second term in (21). Hence the correct initial coherence, $\rho_{23}^{red}(0) = -\alpha\beta$, is regained.

For sufficiently long times, the product of the sinc functions in (21) drives the last pair of terms on the RHS of (21) to zero. The long time asymptote of ρ_{23}^{red} is therefore just the first pair of terms on the RHS of (21), i.e.,

For $\Im << 2U_2$: $$\rho_{23}^{red} \to \rho_{23}^{red}(\infty) = -\alpha\beta + \frac{\alpha\beta}{3U_2^2}\left(1 - \frac{\lambda^2}{4}\right)\sum_{i=1}^{N}\left(P_i\ q_i\right)^2 \tag{26}$$

This expression is only valid when $\Im << 2U_2$ which means that the second term on the RHS of (26) is a modest change to the first (initial) term. This establishes that, for a weak environment, and subject to the simplifications of this toy model, the coherence *in the monomer basis* diminishes little even at arbitrarily long times. The state of the dimer remains close to its initial energy eigenstate, $|1\rangle$, even at long times. The pointer states are close to the energy eigenstates of the isolated dimer, as suggested by Zurek and Paz, [35].

But does this toy model predict complete decoherence, as it should, for a strong environment? The strong environment limit is defined by $\Im >> \aleph > 2U_2$. In this limit we find that the dimer eigenstates including the interaction with the environment approximate to $|1(e)\rangle \approx |hg\rangle$ and $|2(e)\rangle \approx |gh\rangle$. So complete decoherence in the monomer basis is evident. In effect the strong environment destroys the delocalised exciton nature of the dimer states, reducing them back to localised monomer excitations. This confirms that the toy model is capable of predicting full decoherence in the appropriate limit. This is investigated in a little more detail next.

In the strong environment limit, $\Im >> 2U_2$, the coherence decays as,

For $\Im >> 2U_2$: $$\rho_{23}^{red} \approx -\alpha\beta\prod_{j=1}^{N}\mathrm{sinc}\left(\frac{P_j q_j}{\alpha\beta}t\right) \tag{27}$$

Note that the argument of the sinc functions in (27) differs from that of (21).

A crude approximation appropriate in the "less strong" environment limit, when $\Im$ is greater than $2U_2$, but not too much greater, is,

For $\Im = 2U_2 + \delta\Im$: $$\rho_{23}^{red} \approx \rho_{23}^{red}(\text{constant}) - \left[\alpha\beta + \rho_{23}^{red}(\text{constant})\right]\prod_{j=1}^{N}\mathrm{sinc}\left(\frac{P_j q_j}{\alpha\beta}t\right) \tag{28}$$

where the constant term is,

$$\rho_{23}^{red}(\text{constant}) \approx \frac{(1-\chi)}{(1+\chi)^2}\left\{\alpha\beta(\chi - 1) - \left(\beta^2 - \alpha^2\right)\right\} \tag{29}$$

and, $$\chi = 1 + \frac{1}{2}\left[\kappa + \lambda\sqrt{\kappa + 4}\right] \tag{30}$$

where, $$\kappa = \lambda^2 + \frac{3(2U_2)^2}{\sum_{j=1}^{N} P_j^2 q_j^2} \tag{31}$$

The rough approximation, (28), is not valid once $\delta\Im = \Im - 2U_2$ becomes large, and it then gives way to (27), i.e., $\rho_{23}^{red}(\text{constant}) \to 0$.

Figure 1 shows the result of employing the strong environment approximation, (28), based on the 2D Hilbert space (Heitler-London) approximation compared with numerical evaluation of the full 4D formulation. The numerical parameters defining the dimer, their energies and

potentials, are given in Appendix A. The environment parameters are given in the Figure caption. Figure 1 plots the real part of ρ_{23}^{red} against time (in fs). There is reasonably good agreement between the Heitler-London approximation and the 4D formulation, both showing the characteristic sinc-shaped curve. The analytic approximation of Equ.(28) rather underestimates the amplitude of the short-time oscillations in ρ_{23}^{red}. This may be because the contribution of the states $\{|gg\rangle, |hh\rangle\}$, which are ignored in the Heitler-London approximation, are actually significant. However, the salient feature is that the long time behaviour is a non-zero residual coherence ($\rho_{23}^{red} \sim -0.1$ compared with the initial value $\rho_{23}^{red} = -0.42$ corresponding to $\alpha = 0.477$, $\beta = 0.879$).

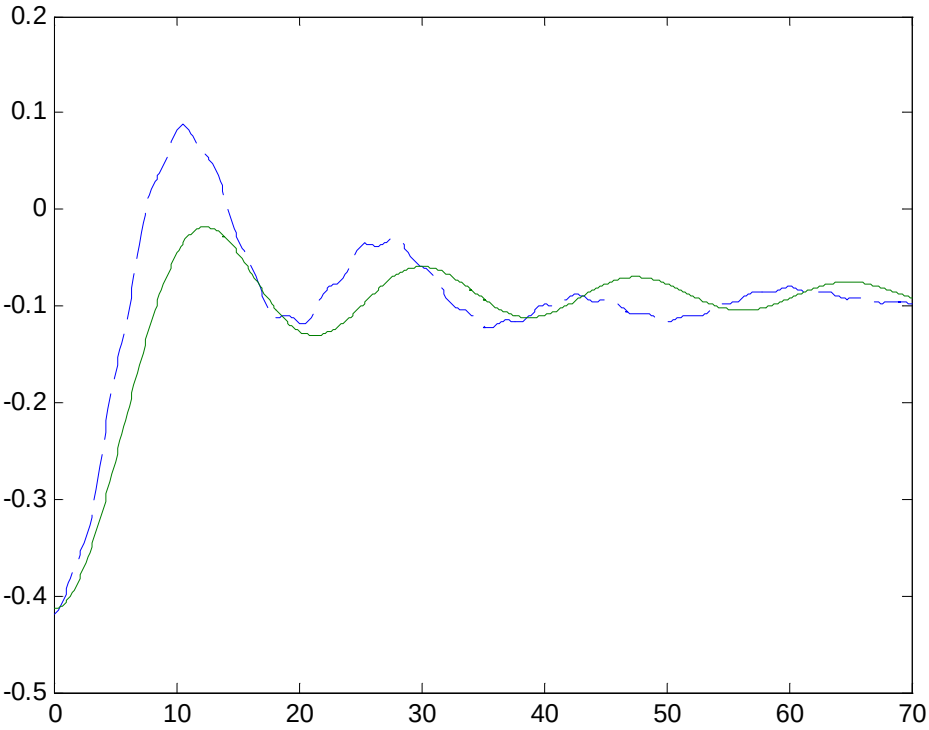

Figure 1: Real part of ρ_{23}^{red} versus time (fs). Illustration of the strong environment analytic approximation of Equ.(28) (green continuous) compared with a numerical evaluation of the 4D formulation of §3 (blue dashed). The dimer parameters are defined in Appendix A. The environment consists of a single 1.8 Debye dipole at position (12,0,0) Angstroms with reference to the dimer coordinate system (see Appendix A), with $\varepsilon_{r,ij}^{e} = 4$. The numerical evaluation used 8000 random orientations of the environment dipole for the trace-out. The sinc function decay of the coherence is clearly evident, but the salient feature is the non-zero residual coherence.

Figure 2 illustrates the weak-environment approximation, (21), for the same dimer parameters, compared with numerical evaluation of the full 4D formulation. The environment parameters are given in the Figure caption. In this case the analytic approximation of Equ.(21) rather exaggerates the amplitude of the short-time oscillations in ρ_{23}^{red}. This may again be because the contribution of the states $\{|gg\rangle, |hh\rangle\}$ is significant. However, the salient feature is that (21) gives a reasonably good account of the residual coherence at long times. The approximation (21) will underestimate the actual residual coherence because, in the strong environment limit, (21) tends to (27) with zero residual coherence.

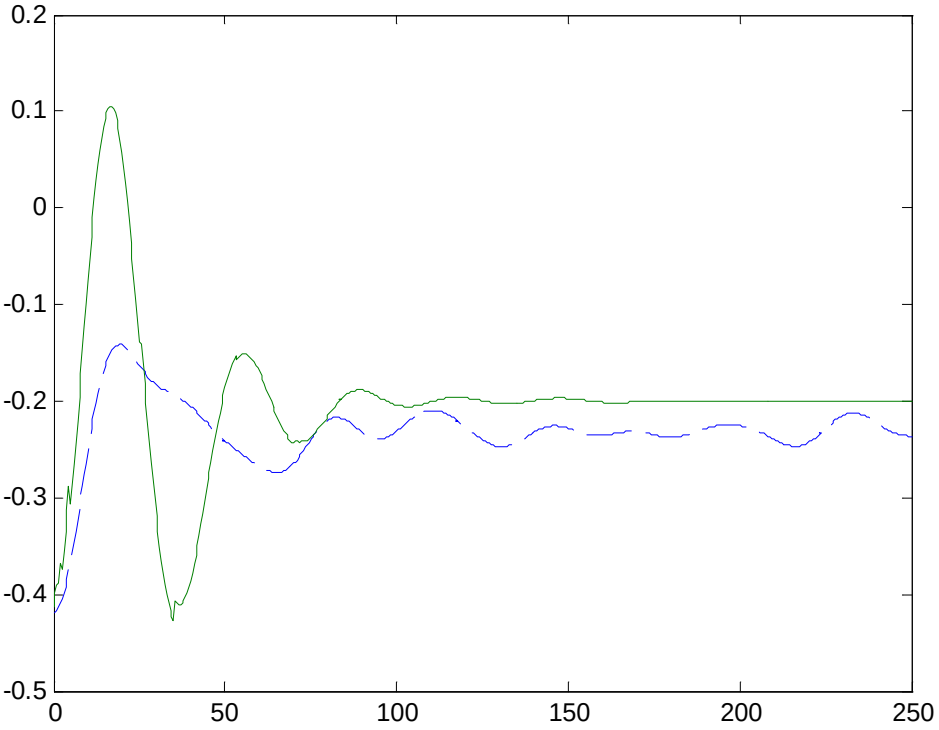

Figure 2: Real part of ρ_{23}^{red} versus time (fs). Illustration of the weak environment analytic approximation of Equ.(21) (green continuous) compared with a numerical evaluation of the 4D formulation of §3 (blue dashed). The dimer parameters are defined in Appendix A. The environment consists of twenty 1.8 Debye dipoles at random positions on a sphere of radius 12 Angstroms with respect to the dimer coordinate system (see Appendix A), with $\varepsilon_{r,ij}^{E} = 4$. The numerical evaluation used 1000 random, uncorrelated orientations of the twenty environment dipoles for the trace-out. The salient feature is the non-zero residual coherence.

5. Models with improved environment states

In this section the environment states are defined rather more realistically, though still highly simplified. The environment is again defined by *N* point dipoles, initially of equal magnitude, *q*. They are placed at homogeneously random positions within a sphere of radius *a* centred on the point midway between the monomers, $\vec{s}_m = (\vec{s}_1 + \vec{s}_2)/2$, but are excluded from spheres of radius *b* centred on each monomer. Hence *b* is the smallest permitted distance between either monomer and any ED. The initial orientations of the EDs are chosen randomly and isotropically in 3D. A large number, N_{states}, of environment states is used to evaluate

numerically the trace-out sum, (14). The N_{states} environment states are constructed by the following process,

(1) For each of the *N* EDs, an uncorrelated random thermal fluctuation in position, $\vec{\Delta}_j$, is generated and the ED positions changed to $\vec{s}'^{e}_j = \vec{s}^{e}_j + \vec{\Delta}_j$;

(2) For each of the *N* EDs, an uncorrelated random thermal fluctuation in dipole magnitude, Δ_{qj}, is generated and the ED dipole magnitudes changed to $q'_j = q + \Delta_{qj}$;

(3) For each of the *N* EDs, the dipole moment is multiplied by either $+1$ or -1 chosen with equal probability in an uncorrelated manner, so that typically about half the EDs have their orientation changed by a 180^o 'flip' for each new environment state generated;

The magnitude and distribution of each of the fluctuations, (1-3) above, are specified in Appendix B.

As regards the crucial issue of the dielectric between the dimer and the EDs, we present results for three different models. The first simply uses the constant $\varepsilon^{e}_{r,ij} = 4$, crudely appropriate for an aqueous environment over very short times. In reality the effective dielectric constant increases to ~80 over some relaxation time (~8 ps), but this dielectric relaxation is not modelled. Note that by using a dielectric constant appropriate for short-times (high frequency), the dimer-environment interaction potential is exaggerated at longer times.

In the second model, $\varepsilon^{e}_{r,ij}$ is treated as a fluctuating parameter and chosen randomly, and uncorrelated, from a flat distribution $\left[\varepsilon^{e}_{r,\min}, \varepsilon^{e}_{r,\max}\right]$. Hence the potential energy due to each ED is evaluated for a different, randomly assigned dielectric constant. Moreover, the dielectric constants for each ED are uncorrelated between environment states. However, the major simplification in both these dielectric models is that the environment state is fixed during the unitary evolution of the dimer state. Dielectric relaxation is not modelled. This is obviously a serious omission.

Dielectric relaxation essentially involves a dynamic change of the state of the environment. The third model therefore includes a number, N_e, of different environment states in the unitary dynamics. For this purpose the environment can be considered as having two components: the point dipoles and the dielectric. The fluctuating state of the point dipoles is treated as described above. The dielectric state is labelled by its effective dielectric constant, $\varepsilon^{e}_{r,ij}$, which for this purpose is now regarded as the same for all EDs.

The Hamiltonian must now be formulated in a Hilbert space of dimension $4N_e$. Each 4×4 block on its diagonal is of the form defined in §3. But we must now also define terms off the block-diagonal. These terms are essential since they allow one dielectric state to dynamically transform into another. No pretence of a realistic model is made at this point. Instead we are content to deploy a rather arbitrary assumption, namely that the off-block-diagonal elements between dielectric states ε_{r1} and ε_{r2} are given by,

$$\left\langle IJ, \varepsilon_{r1} \left| \hat{V}_{env} \right| KL, \varepsilon_{r2} \right\rangle = \left| \left\langle IJ, \varepsilon_{r1} \left| \hat{V}_{env} \right| KL, \varepsilon_{r1} \right\rangle - \left\langle IJ, \varepsilon_{r2} \left| \hat{V}_{env} \right| KL, \varepsilon_{r2} \right\rangle \right| \qquad (32)$$

These terms are therefore defined via (9). Other than the fact that the transition matrix elements are larger the greater is the expected potential energy difference, there is nothing to justify this crude ansatz. However it results in states of different ε_r contributing to the reduced density matrix to a comparable degree. This is the best that can be expected for purely unitary evolution. Actual dielectric relaxation would require a non-unitary dynamic.

In this third model the smallest ε_r is always set to 4 and the largest ε_r is always set to 80. The dimer is prepared in free state $|1\rangle$, as with all models, and the environment is taken to be in the state with $\varepsilon_r = 4$ at $t = 0$. At later times, terms off the block diagonal in the $4N_e \times 4N_e$ density matrix arise due to the transition matrix elements, (32), in the Hamiltonian. The effect of dielectric relaxation is achieved by equating the final 4×4 density matrix for the dimer to the $\varepsilon_r = 80$ term on the block diagonal of the reduced $4N_e \times 4N_e$ density matrix, after renormalizing to unit trace. By this means the effect of dielectric relaxation is modelled in a crude and simplistic fashion without the need to introduce non-unitary terms into the dynamics. The result will be appropriate only for long times (>8 ps).

All numerical results are for the dimer parameters given in Appendix A together with an environment of $N = 100$ EDs contained within a sphere of radius a = 10 Angstroms, each ED having a dipole strength of 1.8 Debyes (e.g., water molecules). The 'exclusion zone' around each monomer is of radius $b = 2$, 3, 4 or 5 Angstroms. The average spacing between EDs is thus ~3.3 Angstroms in any direction. All runs performed the trace-out operation by summing over at least $N_{states} = 100$ randomly generated environment states, and up to 2000 states in some cases to check the stability of the results. The environment fluctuation parameters are intended to be crudely representative of room temperature (see Appendix B).

These dimer parameters give a starting coherence of $\rho_{23}(0) = -\alpha\beta = -0.42$ in all cases. The value of ρ_{23}^{red} at later times is to be compared with this starting value.

Table 2 presents the results for the long-term, asymptotic coherence from the first two models: (i)model 1 with dielectric constant fixed at 4; and, (ii)model 2 with dielectric distributed randomly between $\varepsilon_{r,ij}^{e,\min} = 4$ and $\varepsilon_{r,ij}^{e,\max} = 8$. These are models formulated in a 4D Hilbert space with a constant environment state during unitary evolution. Due to the random distribution of EDs, and their random fluctuations, different results are obtained each time a simulation is run. Each case was run 14 times and the average values, and standard deviations, of the residual $\left|\rho_{23}^{red}\right|$ are summarised in Table 2.

In all cases the residual coherence asymptote was reached within ~100fs, apart from small persistent random fluctuations (due to random sampling). Although Table 2 shows that substantial residual coherence remains, there is also a clear degree of decoherence with respect to the starting value of $|\rho_{23}(0)| = 0.42$. The corresponding decoherence time is thus ~100fs or less, but coherence persists nevertheless.

It can be treacherous to use the off-diagonal components of a density matrix as an entanglement witness (non-zero off-diagonal components will generally occur even for a state with zero entanglement if expressed in an arbitrary basis). Consequently the entanglement of formation (EoF) has also been evaluated for all the above simulations, at a time of 5 ps, using the algorithm due to Wootters, [42]. This is applicable to an arbitrary bipartite density matrix representing a pair of two-level monomers. The results are also given in Table 2. There is essentially a one-to-one correspondence between $\left|\rho_{23}^{red}\right|$ and EoF for this model.

b	$\varepsilon_{r,ij}^{e,\max}$	$\left\|\rho_{23}^{red}\right\|$	EoF	$\varepsilon_{r,ij}^{e,\max}$	$\left\|\rho_{23}^{red}\right\|$	EoF
5	4	0.30 ± 0.02	0.46	8	0.34 ± 0.02	0.58
4	4	0.24 ± 0.03	0.34			
3	4	0.19 ± 0.05	0.23			
2	4	0.11 ± 0.04	0.10	8	0.18 ± 0.06	0.21

Table 2: Summary of residual coherences, expressed as both $\left|\rho_{23}^{red}\right|$ and EoF (entanglement of formation) for models in a 4D Hilbert space with constant environment states. Starting values at t = 0 are $\left|\rho_{23}^{red}\right| = 0.42$ and EoF = 0.77. The error bars are standard deviations over 14 runs.

A key feature of the results in Table 2 is that the residual coherence reduces as the EDs are permitted to approach the monomers more closely, i.e., as b is reduced. This is to be expected since it leads to a greater interaction energy between the dimer and the environment. It suggests that the decoherence characteristics of a given pair of chromophores may be determined primarily by the proximity of the nearest water molecule.

Tables 3 and 4 present the corresponding results for the third model, formulated in $4N_e$ dimensional Hilbert space with an evolving environment-dielectric state. Five different cases were considered, with 2, 6, 10, 20 or 39 active environment states, with dielectric labels as follows,

(i) $N_e = 2$, $\{\varepsilon_r\} = \{4,80\}$

(ii) $N_e = 6$, $\{\varepsilon_r\} = \{4,7,12,20,40,80\}$

(iii) $N_e = 10$, $\{\varepsilon_r\} = \{4,6,8,10,12,16,20,40,60,80\}$

(iv) $N_e = 20$, $\{\varepsilon_r\} = \{4,8,12,16....80\}$

(v) $N_e = 39$, $\{\varepsilon_r\} = \{4,6,8,10,12.....80\}$

In most cases the residual coherence asymptote was reached within ~150fs, but for the largest N_e the steady residual coherence was not reached until after ~700fs.

There is a non-zero residual coherence (ρ_{23}^{red}) in all cases. Its magnitude tends to reduce as the number of environment states involved in the unitary evolution increases. However, the residual ρ_{23}^{red} does not appear to become zero even for large N_e, as illustrated by plotting against $1/N_e$ in Figure 3.

b	$N_e = 2$	$N_{er} = 6$	$N_e = 10$	$N_e = 20$	$N_e = 39$
5	0.24 ± 0.01	0.23 ± 0.01	0.20 ± 0.02	0.14 ± 0.01	0.15 ± 0.01
4	0.26 ± 0.01	0.19 ± 0.01	0.17 ± 0.03	0.12 ± 0.01	0.13 ± 0.01
3	0.16 ± 0.03	0.14 ± 0.03	0.12 ± 0.01	0.10 ± 0.01	0.12 ± 0.01
2	0.10 ± 0.02	0.09 ± 0.02			0.12 ± 0.01

Table 3: Summary of residual coherences, $\left|\rho_{23}^{red}\right|$, for models in a Hilbert space of dimension $4N_e$ where N_e is the number of environment states taking part in the unitary evolution. The starting value is $\left|\rho_{23}^{red}\right| = 0.42$ at t = 0. The error bars are standard deviations over 7 runs.

Table 4 and Figure 3 also give the residual entanglement of formation. This is also non-zero in most cases, but the EoF appears to become zero for large N_e if $b \leq 3$ Angstrom. For environment dipoles constrained to lie at 4 Angstroms distance, or greater, there appears to be a non-zero residual entanglement between the monomers even for large N_e.

b	$N_e = 2$	$N_e = 6$	$N_e = 10$	$N_e = 20$	$N_e = 39$
5	0.32 ± 0.07	0.34 ± 0.04	0.22 ± 0.05	0.08 ± 0.04	0.10 ± 0.04
4	0.36 ± 0.04	0.18 ± 0.04	0.18 ± 0.08	0.06 ± 0.03	0.06 ± 0.03
3	0.13 ± 0.09	0.12 ± 0.07	0.07 ± 0.05	0.01 ± 0.01	0.01 ± 0.01
2	0.04 ± 0.04	0.02 ± 0.02			0

Table 4: Summary of residual entanglement (EoF) for models in a Hilbert space of dimension $4N_e$ where N_e is the number of environment states taking part in the unitary evolution. The starting value is EoF = 0.77 at t = 0. The error bars are standard deviations over 7 runs.

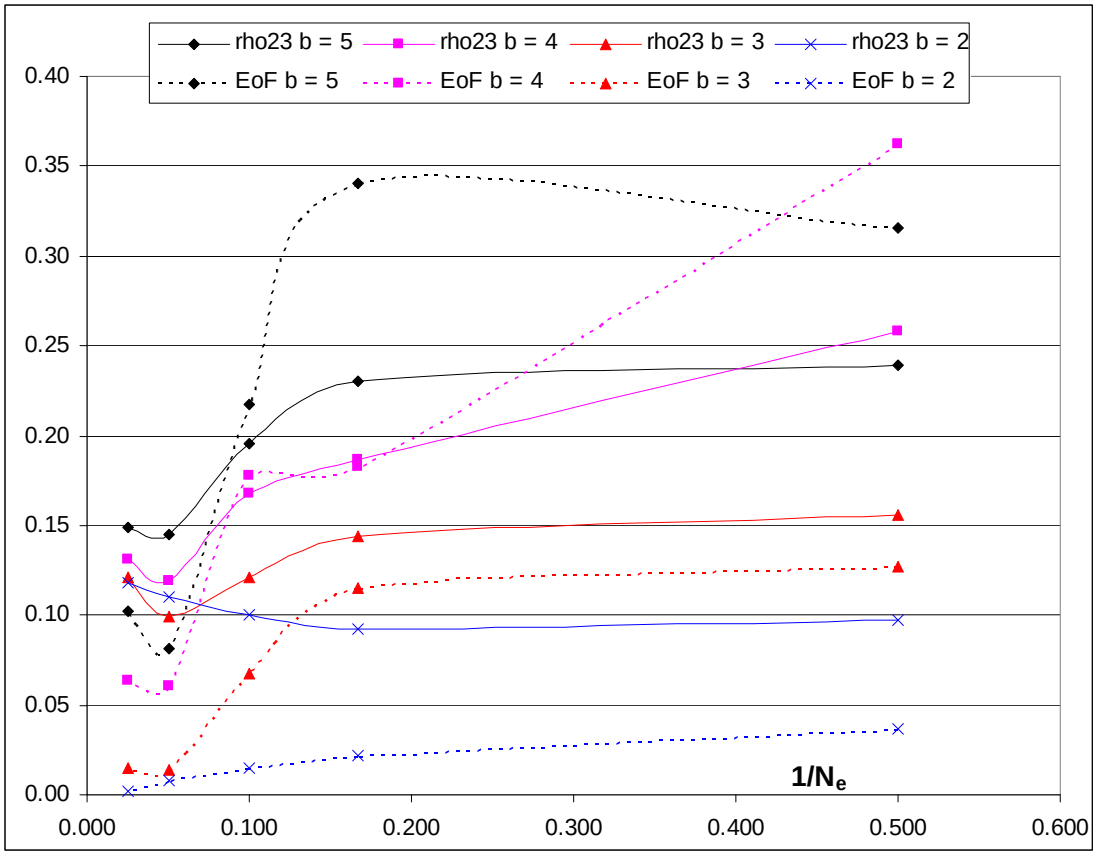

Figure 3: Long-time residual coherence, absolute magnitude of ρ_{23}^{red}, and entanglement of formation (EoF) versus reciprocal of the number of environment states, $1/N_e$, for four values of b, the smallest permitted distance between the monomers and the environment dipoles (Angstrom). The dimer parameters are defined in Appendix A and the environment parameters in Appendix B. The environment consists of one hundred 1.8 Debye dipoles at random positions within a sphere of radius $a = 10$ Angstroms centred on the mid-point between the monomers (see §5). The numerical evaluation used 100 random, uncorrelated states of the hundred environment dipoles for the trace-out, where the distribution of states is defined in §5 and Appendix B.

6. Conclusions

A case has been presented in favour of the notion that coherence and entanglement between monomers may persist indefinitely if the inter-monomer coupling is strong compared with the coupling to the environment. This is expected on general grounds, following Zurek and Paz, [35], who argue that if the spacing of the energy levels of an isolated system exceeds the frequencies present in the environment (i.e., if $2\Delta > \hbar\omega_c$), then the pointer states will approximate to the energy eigenstates of the system. The indefinite persistence of coherence has previously been reported for appropriate parameter ranges and specific models by Reina et al, [32], and Jun-Hong An et al, [33], though not in the context of photosynthesis.

The obvious question is why is persistent coherence not observed in the many models of decoherence in photosynthetic systems reported in the literature? In the case of strictly Markovian dynamics, e.g., [8, 9], this is simply because exponential decay of the coherences is ensured by the Lindblad master equation. The Lindblad master equation is the most general Markovian dynamic equation respecting the required mathematical properties of the density matrix. It has constant dephasing rates which generically integrate to give exponential decays of coherence (excepting peculiar circumstances such as decoherence-free subspaces).

Many of the models in the literature, recognising the shortcomings of the Markovian assumption, use some form of non-Markov model, e.g., [10-12, 28, 30]. However, if the real parts of the parameters multiplying the density matrix on the RHS of a master equation are assumed time-independent, then exponential decay of the coherences will again be the generic behaviour. This is a common assumption, the constants in question being estimated by relating them back to relevant relaxation times. However, non-Markovian behaviour can lead to a time-dependent decay parameter which vanishes after a certain period, $\gamma_{ab}(t \to \infty) \to 0$, which results in persistent non-zero off-diagonal terms in the reduced density matrix. In the present paper we have avoided the use of a master equation, with the associated, rather *ad hoc*, non-unitary terms, opting instead for a purely unitary dynamics.

Finally, we note that independent boson models are bound to predict that coherences decay to zero, since these models have zero internal coupling ($\Delta = 0$) and hence the environmental interaction is always stronger. However, in the context of the spin boson model, for which $\Delta \neq 0$, Thorwart et al, [31], have observed that the decay rate of the negativity decreases sharply with diminishing ω_c when $\omega_c < \Delta$, consistent with our contention.

The purpose of the present paper has been to illustrate with the aid of toy models that the indefinite persistence of coherence is not exotic but can arise very simply for strongly coupled dimers. It must be emphasised that the toy models themselves are not to be taken seriously as models of any biological system, being naïve in many respects. In particular the unitary dynamics makes it problematical to model dielectric relaxation of an aqueous environment. However, our intention has been only to point out that current modelling techniques may under-estimate coherence and entanglement in strongly coupled systems by artificially constraining their long term behaviour to decay to zero when this may not be the case.

Appendix A – Dimer parameters used in all the models

In all cases the dimer consists of identical monomers which have a dipole strength of 5 Debyes in their ground state and 11.1 Debyes in their excited state. Their transition dipole between these states is 7.54 Debyes. The first monomer has position vector (10,0,0) Angstroms with respect to some origin, and its ground state dipole is aligned with the x-axis. The orientation of its excited state dipole is given by direction cosines $\left(1/\sqrt{2}, 1/\sqrt{2}, 0\right)$ and the orientation of its transition dipole is (0.85,0.52,0). The position and dipole orientations of the second monomer are obtained by rotating the first anti-clockwise about the z-axis through the origin by 29^o. This results in the monomers being separated by 5 Angstroms. These magnitudes are intended to be crudely representative of adjacent pigment molecules in a

photosynthetic unit, but not specific to any system nor intended to be accurate. The dielectric of the material between the monomers, $\varepsilon_{r,12}$, is taken to be 2 in all cases.

Appendix B – Environment parameters used in the models of §5

B.1 Fluctuations in Environment Dipole (ED) Positions

Assuming classical simple harmonic motion, the mean amplitude of vibration is $\langle\Delta\rangle = \sqrt{2kT/S}$, where S is the stiffness of the restoring force. Assuming an interaction between neighbouring molecules given by an potential energy of (say) $E = \frac{A}{x^{12}} - \frac{B}{x^6}$, where x is the distance between the neighbouring molecules, the stiffness is found as $S = \frac{156A}{x^{14}} - \frac{42B}{x^8}$ and the equilibrium distance is $x = \left(\frac{2A}{B}\right)^{1/6}$. Taking the inter-molecular force to be a hydrogen bond of typical length ~1.9 Angstroms and energy ~0.2eV, the parameters are determined to be A = 442 and B = 18.8 in units of Angstroms and eV. This results in a mean vibration amplitude of $\langle\Delta\rangle = 0.11$ Angstroms at T = 300K. The thermal distribution of amplitudes amongst the N EDs is thus,

$$P(\Delta) = \frac{2}{\pi\langle\Delta\rangle}\exp\left\{-\frac{1}{\pi}\left(\frac{\Delta}{\langle\Delta\rangle}\right)^2\right\} \qquad \text{(B.1)}$$

Each of the three coordinate directions takes an associated vibration amplitude from the same distribution, (B.1). Each randomly generated environment state places the EDs at the extremity of their classical vibrational motion.

B.2 Fluctuations in ED Magnitudes

The fluctuations in the dipole magnitudes are assumed to result from intra-molecular vibration of hydrogen atoms. The mean amplitude at frequency f is $\frac{1}{\pi f}\sqrt{\frac{kT}{2M}}$, where M is the proton mass. Assuming the infrared absorption peak of water, at 2900 nm, this amplitude is 0.034 Angstroms at T = 300K. This is 3.5% of the mean OH bond length of 0.96 Angstroms. Hence it is assumed that the amplitude of the dipole fluctuations is ±3.5% of the nominal dipole strength of water (1.8 Debyes), i.e., a mean fluctuation amplitude of $\langle\Delta_q\rangle = 0.064$ Debyes. The thermal distribution of dipole magnitude fluctuations is thus,

$$P(\Delta_q) = \frac{2}{\pi\langle\Delta_q\rangle}\exp\left\{-\frac{1}{\pi}\left(\frac{\Delta_q}{\langle\Delta_q\rangle}\right)^2\right\} \qquad \text{(B.2)}$$

B.3 Fluctuations in ED Orientations

The hydrogen bonds between water molecules create a partial framework which suppresses their free rotation. Nevertheless, gross rotations of water molecules occur as hydrogen bonds break and re-form onto a different neighbour. This is modelled here simply as a sign reversal of the dipole (i.e., a 180^o 'flip'). In reality such flips are unlikely to arise in timescales of less than ~100 fs, and it is probably an exaggeration of their effect to assume complete randomisation of their orientations (as here) for periods of less than ~1 ps at least. This is a particularly significant exaggeration of the influence of the environment because, whilst the fluctuations in EM position and dipole magnitude cause a fractional change in each dimer-EM potential, the flips of orientation reverse the sign of the potential energy (causing a 200% change).

References

[1] Savikhin S, Buck D R and Struve W S 1997 Oscillating anisotropies in a bacteriochlorophyll protein: evidence for quantum beating between exciton levels *Chem. Phys.* **223** 303

[2] Herek J L, Wohlleben W, Cogdell R J, Zeidler D and Motzkus M 2002 Quantum control of energy flow in light harvesting *Nature* **417** 533

[3] Engel G S, Calhoun T R, Read E L, Ahn T K, Mancal T, Cheng Y C, Blankenship R E and Fleming G R 2007 Evidence for wavelike energy transfer through quantum coherence in photosynthetic systems *Nature* **446** 782

[4] Lee H, Cheng Y C and Fleming G R 2007 Coherence dynamics in photosynthesis: protein protection of excitonic coherence *Science* **316** 1462

[5] Collini E and Scholes G D 2009 Coherent intrachain energy migration in a conjugated polymer at room temperature *Science* **323** 369

[6] Collini E, Wong C Y, Wilk K E, Curmi P M G, Brumer P and Scholes G D Coherently wired light-harvesting in photosynthetic marine algae at ambient temperature *Nature* **463** 644

[7] Panitchayangkoon G, Hayes D, Fransted K A, Caram J R, Harel E, Wen J, Blankenship R E and Engel G S 2010 Long-lived quantum coherence in photosynthetic complexes at physiological temperature *Proc. Natl. Acad. Sci.* **107** 12766

[8] Mohseni M, Rebentrost P, Lloyd S and Aspuru-Guzik A 2008 Environment-assisted quantum walks in photosynthetic energy transfer *J. Chem. Phys.* **129** 174106

[9] Rebentrost P, Mohseni M, Kassal I, Lloyd S and Aspuru-Guzik A 2009 Environment-assisted quantum transport *New J. Phys.* **11** 033003

[10] Caruso F, Chin A W, Datta A, Huelga S F and Plenio M B 2010 Entanglement and entangling power of the dynamics in light-harvesting complexes *Phys. Rev. A* **81** 062346

[11] Plenio M B and Huelga S F 2008 Dephasing assisted transport: quantum networks and biomolecules *New J. Phys.* **10** 113019

[12] Liang X T 2010 Excitation energy transfer: study with non-Markovian dynamics *Phys. Rev. E* **82** 051918

[13] Fassioli F, Nazir A and Olaya-Castro A 2010 Quantum state tuning of energy transfer in a correlated environment *J. Phys. Chem. Lett.* **1** 2139

[14] Knox R S 1996 Electronic excitation transfer in the photosynthetic unit: reflections on work of William Arnold *Photosynth. Res.* **48** 35

[15] Leegwater J A 1996 Coherent versus incoherent energy transfer and trapping in photosynthetic antenna complexes *J. Phys. Chem.* **100** 14403

[16] Yang M and Fleming G R 2002 *Chem. Phys.* **275** 355

[17] Scholes G D 2003 *Annu. Rev. Phys. Chem.* **54** 57

[18] Novoderezhkin V I, Palacios M A, van Amerongen H and van Grondelle R 2004 *J. Phys. Chem. B* **108** 10363

[19] Jang S, Newton M D and Silbey R J 2004 *Phys. Rev. Lett.* **92** 218301

[20] Sener M K, Park S, Lu D, Damjanovic A, Ritz T, Fromme P and Schulten K 2004 *J Chem. Phys.* **120** 11183

[21] Gilmore J and McKenzie R H 2006 Criteria for quantum coherent transfer of excitons between chromophores in a polar solvent *Chem. Phys. Lett.* **421** 266

[22] Gilmore J and McKenzie R H 2005 Spin-boson models for quantum decoherence of electronic excitations of biomolecules and quantum dots in a solvent *J. Phys.: Condens. Matter* **17** 1735

[23] Gilmore J and McKenzie R H 2008 Quantum dynamics of electronic excitations in biomolecular chromophores: role of the protein environment and solvent *J. Phys. Chem. A* **112** 2162

[24] Olaya-Castro A, Lee C F, Olsen F F and Johnson N F 2008 *Phys. Rev. B* **78** 085115

[25] Rebentrost P, Mohseni M, and Aspuru-Guzik A 2009 Role of quantum coherence in chromophoric energy transport, *J. Phys. Chem. B* **113** 9942

[26] Ishizaki A and Fleming G R 2009 On the adequacy of the Redfield equation and related approaches to the study of quantum dynamics in electronic energy transfer *J. Chem. Phys.* **130** 234110

[27] Ishizaki A and Fleming G R 2009 Unified treatment of quantum coherent and incoherent hopping dynamics in electronic energy transfer: reduced hierarchy equations approach *J. Chem. Phys.* **130** 234111

[28] Ishizaki A and Fleming G R 2009 Theoretical examination of quantum coherence in photosynthetic systems at physiological temperature *P. Natl. Acad. Sci.* **106** 17255

[29] Ishizaki A and Fleming G R 2010 Quantum superpositions in photosynthetic light harvesting: delocalization and entanglement *New J. Phys.* **12** 055004

[30] Sarovar M, Ishizaki A, Fleming G R and Whaley K B 2010 Quantum entanglement in photosynthetic light harvesting complexes *Nature Physics* **6** 462

[31] Thorwart M, Eckel J, Reina J H, Nalbach P and Weiss S 2009 Enhanced quantum entanglement in the non-Markovian dynamics of biomolecular excitons *Chem. Phys. Lett.* **478** 234

[32] Reina J H, Quiroga L and Johnson N F 2002 Decoherence of quantum registers *Phys. Rev. A* **65** 032326

[33] An J H, Yeo Y, Zhang W M, Oh C H 2009 Entanglement oscillation and survival induced by non-Markovian decoherence dynamics of entangled squeezed-state, *J. Phys. A: Math. Theor.* **42** 015302

[34] Zurek W H 2003 Decoherence, einselection, and the quantum origins of the classical *Rev. Mod. Phys.* **75** 715

[35] Zurek W H and Paz J P 1999 Quantum limit of decoherence: environment induced superselection of energy eigenstates *Phys.Rev.Lett.* **82** 5181

[36] Paz J P and Zurek W H 1999 Environment-induced decoherence and the transition from quantum to classical, *Lectures at 72nd Les Houches Summer School on Coherent Matter Waves, July-August 1999*. arXiv:quant-ph/0010011

[37] Hu X, Ritz T, Damjanovic A and Schulten K 1997 *J. Phys. Chem. B* **101** 3854

[38] Cho M, Vaswani H M, Brixner T, Stenger J and Fleming G R 2005 Exciton analysis in 2D electronic spectroscopy *J Phys Chem B* **109** 10542

[39] Adolphs J and Renger T 2006 How proteins trigger excitation energy transfer in the FMO complex of green sulfur bacteria *Biophys. J.* **91** 2778

[40] Read E L, Schlau-Cohen G S, Engel G S, Wen J, Blankenship R E and Fleming G R 2008 Visualization of excitonic structure in the Fenna-Matthews-Olson photosynthetic complex by polarization-dependent two-dimensional electronic spectroscopy *Biophys. J.* **95** 847

[41] Renger T and Marcus R A 2002 On the relation of protein dynamics and exciton relaxation in pigment-protein complexes: an estimation of the spectral density and a theory for the calculation of optical spectra *J. Chem. Phys*. **116** 9997

[42] Wootters W K 1998 Entanglement of formation of an arbitrary state of two qubits *Phys. Rev. Lett*. **80** 2245

[43] Wong V and Gruebele M 1999 How does vibrational energy flow fill the molecular state space? *J. Phys. Chem. A* **103** 10083

[44] Wong V and Gruebele M 2001 Nonexponential dephasing in a local random matrix model *Phys.Rev. A* **63** 022502

[45] Sinha S 1997 Decoherence at absolute zero *Phys.Lett. A* 228 1